Applied Energy 251 (2019) 113357

Contents lists available at ScienceDirect

Applied Energy

journal homepage: www.elsevier.com/locate/apenergy

Facilitating static firm frequency response with aggregated networks of commercial food refrigeration systems

A. Postnikov[a,*,1], I.M. Albayati[a], S. Pearson[b], C. Bingham[a], R. Bickerton[a], A. Zolotas[a,2]

[a] School of Engineering, University of Lincoln, Brayford Pool, Lincoln LN6 7TS, UK
[b] Lincoln Institute of Agri-Food Technology, University of Lincoln, Brayford Pool, Lincoln LN6 7TS, UK

HIGHLIGHTS

- A simulation model is developed to analyse aggregated refrigeration loads.
- Real refrigeration data from small and large stores are used for validation.
- Firm frequency response is delivered as virtual defrost with suction pressure offset.
- The proposed scenario of delivering frequency response is with a 30 s delay.

ARTICLE INFO

Keywords:
Thermostatically controlled loads
Firm frequency response
Demand side management
Refrigeration systems
Computer simulation
Modelling

ABSTRACT

Aggregated electrical loads from massive numbers of distributed retail refrigeration systems could have a significant role in frequency balancing services. To date, no study has realised effective engineering applications of static firm frequency response to these aggregated networks. Here, the authors present a novel and validated approach that enables large scale control of distributed retail refrigeration assets. The authors show a validated model that simulates the operation of retail refrigerators comprising centralised compressor packs feeding multiple in-store display cases. The model was used to determine an optimal control strategy that both minimised the engineering risk to the pack during shut down and potential impacts to food safety. The authors show that following a load shedding frequency response trigger the pack should be allowed to maintain operation but with increased suction pressure set-point. This reduces compressor load whilst enabling a continuous flow of refrigerant to food cases. In addition, the authors simulated an aggregated response of up to three hundred compressor packs (over 2 MW capacity), with refrigeration cases on hysteresis and modulation control. Hysteresis control, compared to modulation, led to undesired load oscillations when the system recovers after a frequency balancing event. Transient responses of the system during the event showed significant fluctuations of active power when compressor network responds to both primary and secondary parts of a frequency balancing event. Enabling frequency response within this system is demonstrated by linking the aggregated refrigeration loads with a simplified power grid model that simulates a power loss incident.

1. Introduction

The drive towards low carbon economies with electrical power generation provided by increased proportions of renewables (wind/solar PV) is increasing pressure on national power grid infrastructure. In addition, reduced inertia, as a consequence of renewable loads, increases grid maintenance complexity. To mitigate these impacts, increased emphasis is now placed on demand side response mechanisms (DSR) that aim to stabilise load by modifying demand rather than generation supply. Measures include financial incentives for industry to modify demand, typically load shedding, in response to in-balances on the grid [1]. Given the scale of these challenges, it is clear that the successful implementation of DSR will require the aggregation of loads from multiple industrial processes [2,3].

* Corresponding author.
E-mail addresses: a.postnikov@ucl.ac.uk (A. Postnikov), ialbayati@lincoln.ac.uk (I.M. Albayati), spearson@lincoln.ac.uk (S. Pearson), cbingham@lincoln.ac.uk (C. Bingham), rbickerton@lincoln.ac.uk (R. Bickerton), argyrios.zolotas@cranfield.ac.uk (A. Zolotas).
[1] Address: Dept of Civil, Environ & Geomatic Eng, University College London, Gower Street, London WC1E 6BT, UK.
[2] Address: School of Aerospace, Transport and Manufacturing, Cranfield University, Cranfield, Bedfordshire MK43 0AL, UK.

https://doi.org/10.1016/j.apenergy.2019.113357
Received 29 January 2019; Received in revised form 7 April 2019; Accepted 16 May 2019

Nomenclature

A	surface area (m^2)
α, β	empirical constants for refrigerator probes
$\dot{Q}$	heat flow (W)
ρ	density ($kg\,m^{-3}$)
U	overall heat transfer coefficient ($W\,m^{-2}\,K^{-1}$)
m	mass (kg)
V	volume (m^3)
Cp	specific heat capacity ($J\,kg^{-1}\,K^{-1}$)
CPT	calculated product temperature (°C)
$\dot{m}$	mass flow rate ($kg\,s^{-1}$)
h	enthalpy ($J\,kg^{-1}$)
$\dot{V}$	volume flow rate ($m^3\,s^{-1}$)
T	temperature (°C)
P	pressure (bar)
$\dot{W}$	power (W)
η_{me}	mechanical efficiency
η_{vol}	volumetric efficiency
[OD]	expansion valve opening degree
K_v	flow factor ($m^3\,h^{-1}\,bar^{-0.5}$)
SG	specific gravity
HT	high temperature (chillers)
LT	low temperature (freezers)
pr	product
amb	ambient indoor temperature
s	suction
c	compressor
e	evaporator
ic/oc	compressor inlet/outlet
ref	refrigerant

One of the standard DSR mechanisms is static Firm Frequency Response (FFR) where load is shed when the grid frequency drops below a low frequency (LF) trigger. A static FFR event is typically divided into two transitions as illustrated in Fig. 1. In the first transition called primary FFR, the industry has to shed the load rapidly (full output within 10 s) and hold off for further 20 s, while for the second transition the load can be held off for 30 min (i.e. secondary FFR) with full output within 30 s [4]. Primary FFR is aimed at arresting frequency deviations from the nominal, while secondary FFR is performed to contain and partially recover the frequency after the fall has been arrested [5,6].

2. Demand side response and refrigeration systems

Refrigeration and HVAC systems have been proposed for wide scale incorporation into DSR; this is because the thermal inertia within refrigeration systems may maintain the effective performance of the device when electrical load is reduced [7]. These devices are typically thermally buffered (e.g. by food) and might withstand short term (0–30 min) loss of operation. In addition, individual units can consume significant amounts of power (5–20 kW)[8]. With the UK National Grid looking toward contract values of > 10 MW for load shedding events, a large number of refrigeration assets need to be aggregated. Loads of this scale are easily obtainable, the Carbon Trust indicate that refrigeration and HVAC consumes c.14% of the UK's electricity. In addition, the food industry is the UK's largest manufacturing sector, accounting for £188 bn of consumer expenditure and 18% of total UK energy consumption. The food retailing sector alone uses c. 12 TW h of energy per annum and accounts for 3.4% of total electrical consumption, within this c. 29% is used to power in store refrigeration units [9]. The successful integration of food refrigeration systems into DSR mechanisms would have national and internationally relevant impact.

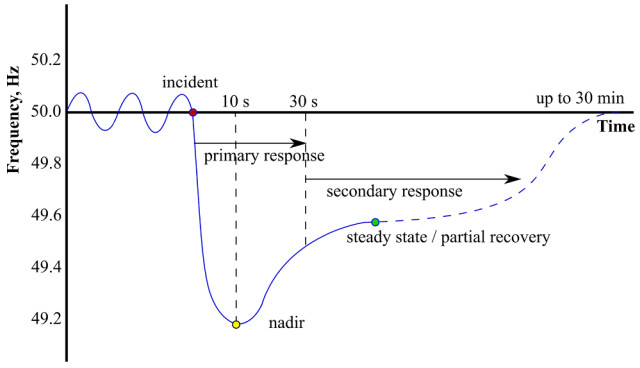

Fig. 1. Frequency response overview (National Grid).

Food refrigeration networks can comprise significant numbers of assets; a typical large supermarket retailer can have over 100,000 refrigeration cases. Many food retail refrigeration systems use large centralised packs containing compressor sets that feed multiple food refrigeration cases. Due to this system complexity, the simplest approach to DSR, shutting down the whole pack, is not available for large food refrigeration systems. This is because on full pack shut down control is lost to all the food cases linked to the centralised compressor system. These cases may be holding different food stuffs at a range of set point temperatures. Food safety would be compromised if temperature in any one case is allowed to increase in an uncontrolled manner. A safer approach is to proportionately reduce compressor function within a pack during a DSR event, for example by stepping down a set number of compressors in a pack but leaving some operational to ensure a flow of refrigerant to high risk cases. This approach also mitigates the risk of refrigerant condensing within the system and associated damage to compressors. In addition, for food systems, great care is required to ensure that temperature in a case does not exceed legally defined set-points. During an FFR event managed safe temperature control can be accomplished by exploiting the thermal inertia (mass) in a case.

Previous studies have identified issues of post DSR event power synchronization that create high transient demands by refrigeration systems [10]. Whilst control and protection devices on power system networks can work to minimize power fluctuations, synchronization could compromise the stability of the grid and increase network failure risks [11]. For small groups of domestic refrigerators, computationally demanding stochastic decentralized control has been proposed to ameliorate the effects of these power oscillations [12,13]. Several studies addressed the importance of numerical weather predictions to forecast the load by assets across the country [14,15]. Pre-cooling of refrigeration assets for enhancing load shift was investigated for domestic appliances in [16]. An approach for implementing a dynamic frequency trigger for grid balancing services was discussed in [17] for domestic refrigeration, with an improved control scheme proposed in [18] for heat pumps.

Safe delivery of FFR in food refrigeration systems requires (i) a control approach that minimises engineering risk to the compressor (ii) food safety management enabled by real time forecasts of the duration an individual case can be shut down before temperature exceeds a critical food safety limit [19], (iii) system recovery approaches that avoid operational synchronisation of refrigerator compressors when the load is restored, (iv) the development of a real time candidacy algorithm that can aggregate responses that are available for frequency balancing.

Here, the authors present a study that addresses the delivery of static FFR as a virtual defrost. The authors approach is demonstrated

via numerical simulations of large refrigeration pack networks with particular emphasis on the aggregated response of 150 and 300 packs with all available assets. The presented simulation model was calibrated and validated via experimental data gathered on a typical centralised pack refrigeration system at the Refrigeration Research Centre in Riseholme, Lincoln (Fig. 2). Moreover, additional experimental data are provided from a large operational retail store with six compressor packs that were subject to a FFR DSR event.

3. Modelling aspects

A typical temperature controller in retail refrigeration systems can operate in two modes: the first is characterised by conventional hysteresis control where expansion valves that provide refrigerant into evaporator coils are closed when the temperature hits the lower boundary, and fully open once the temperature rises beyond a set boundary; the second is modulation where the temperature is maintained close to the set-point value at all times by dynamically adjusting the degree of opening of the expansion valve. Compressor controllers are set to maintain a desired suction pressure in both high temperature (HT, non freezing case operation temperatures) and low temperature (LT for cases operating at temperatures below freezing) suction lines.

The refrigeration cycle is simulated by calculating the properties of the refrigerant at each point of the refrigeration process, such as evaporation, compression and expansion. Temperature of the product T_{pr} and temperature of the air inside a case T_{air} are modelled using first-order heat transfer dynamics, as follows [20,21]:

$$\dot{T}_{pr} = -\frac{1}{m_{pr} Cp_{pr}} \dot{Q}_{pr} \tag{1}$$

$$\dot{T}_{air} = \frac{1}{m_{air} Cp_{air}} (\dot{Q}_{pr} + \dot{Q}_{amb} - \dot{Q}_e) \tag{2}$$

where m and Cp with the corresponding subscripts denote the mass and the specific heat capacity, $\dot{Q}_{pr}$ is the heat transfer between the product and the air inside the case, $\dot{Q}_{amb}$ is the heat load from the environment, and $\dot{Q}_e$ is the cooling capacity. Heat transfer rates [22,23] for Eqs. (1) and eqtair) are:

$$\dot{Q}_{pr} = U_{pr} A_{pr} (T_{pr} - T_{air}) \tag{3}$$

$$\dot{Q}_{amb} = U_{amb} A_{amb} (T_{amb} - T_{air}) \tag{4}$$

$$\dot{Q}_e = U_e A_e (T_{air} - T_e) \tag{5}$$

where U and A with the corresponding subscripts are the overall heat transfer coefficient and the surface area, T_{amb} is the ambient indoor temperature, and T_e is the evaporation temperature. T_e depends on the suction pressure P_s and is calculated from the NIST reference fluid thermodynamic and transport properties database referred to as REFPROP [24].

Temperature monitoring is usually performed by tracking the values of air-off and air-on probes installed at the back and the front of a case correspondingly, as well as the value of CPT (calculated product temperature) – a filtered mean, based on readings from the two probes. An illustration of temperature time histories recorded at the test site from two different HT refrigeration cases is presented in Fig. 3. In Fig. 3a the case is operating in hysteresis mode, whilst the case shown in Fig. 3b is controlled by a modulating valve. In the presented simulation model, readings from the two probes are modelled as:

$$T_{air-off} = \alpha T_{air} + (1 - \alpha) T_e \tag{6}$$

$$T_{air-on} = \beta T_{air} + (1 - \beta) T_{amb} \tag{7}$$

where α and β are empirical coefficients that characterise the type of case (air curtain, doors), its location in the store, etc. The schematic of refrigeration case is illustrated in Fig. 4.

Due to an amount of boiling refrigerant in an evaporator coil, it is

Fig. 2. Refrigeration cases at the Refrigeration Research Centre in Riseholme.

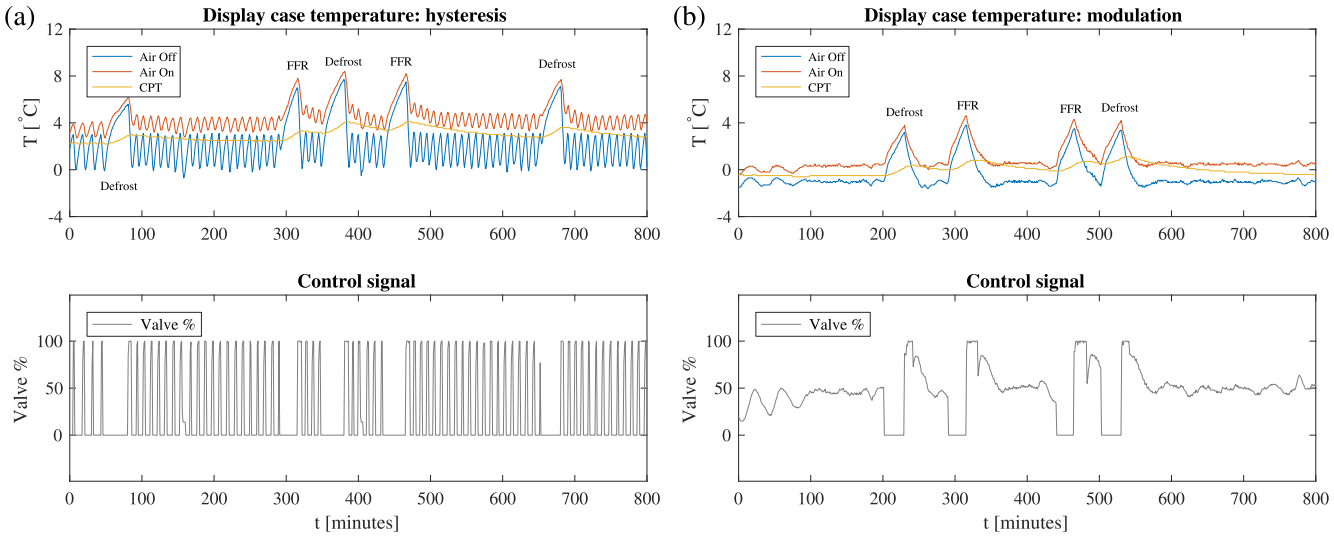

Fig. 3. Experimental data from Refrigeration Research Centre in Riseholme: temperature time histories of refrigeration cases. Simulated FFR is delivered as an unscheduled defrost. (a) Temperature profile of HT case on hysteresis control; (b) temperature profile of HT case on modulation control.

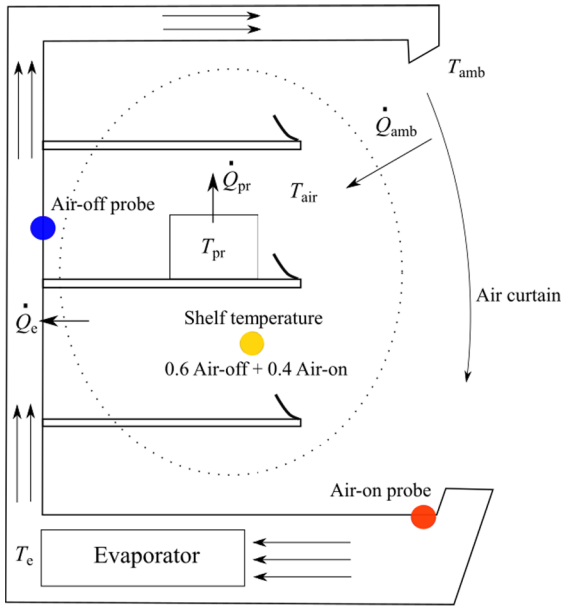

Fig. 4. Refrigeration case schematic.

assumed that a refrigeration effect will remain for a limited amount of time when the expansion valve state is changed from open to closed. Thus, the heat transfer coefficient UA_e is modelled as a linear function of the mass of refrigerant m_{ref} in the evaporator [25]. Refrigerant accumulation in the coil is described by the mass balance in a control volume:

$$\frac{dm_{ref}}{dt} = \dot{m}_{in} - \dot{m}_{out} \tag{8}$$

where $\dot{m}_{in}$ and $\dot{m}_{out}$ are the mass flow rates in [26,27] and out of [28] the evaporator correspondingly, and are as follows:

$$\dot{m}_{in} = [OD] K_v \rho_{ref} \sqrt{\frac{\Delta P}{SG_{ref}}} \tag{9}$$

$$\dot{m}_{out} = \frac{1}{h_{out} - h_{in}} \dot{Q}_e \tag{10}$$

where [OD] is the valve opening degree, K_v is the flow factor of the AKV valve (adaptive control valves by Danfoss, used in tests at the Refrigeration Research Centre), ρ_{ref} is the entering liquid density [29], ΔP is the pressure drop across the valve, SG_{ref} is the specific gravity of the refrigerant, h_{in} is the enthalpy at the inlet of the evaporator, and h_{out} is the enthalpy at the outlet of the evaporator. The type of refrigerant used at the test site and in the model is R407F. It is assumed that $\dot{m}_{out}$ is 100% dry vapour. Superheat T_{sh} is assumed to be constant. It occurs when the vapor is heated above its boiling point in the evaporator. Similarly, subcooling occurs when condensed refrigerant is cooled below the temperature at which it turns into a liquid.

Suction pressure dynamics are related to the accumulation rate of the refrigerant in the suction line [22]. By applying the chain rule, the derivative of density with respect to time in a control volume can be written as [30]

$$\frac{d\rho}{dt} = \left(\frac{\partial \rho}{\partial P}\right)_T \frac{dP}{dt} + \left(\frac{\partial \rho}{\partial T}\right)_P \frac{dT}{dt} \tag{11}$$

and assuming constant superheat, the pressure dynamics in the suction line can be derived from the mass balance and modelled as follows [31]:

$$\left(\left(\frac{\partial \rho_s}{\partial P_s}\right)_{T_e+T_{sh}} \frac{dP_s}{dt}\right) V_s = \sum_{i=1}^{n} \dot{m}_{out}^{i} - \rho_s \sum_{k=1}^{N_c} \eta_{vol}^{k} \dot{V}_k \tag{12}$$

where $\dot{m}_{out}^{i}$ is the mass flow rate from the i-th case, V_s is the volume of the suction line, ρ_s is the density of the refrigerant in the suction line, $\dot{V}_k$ is the volume displacement rate of the k-th compressor in the pack, η_{vol}^{k} is the volumetric efficiency of the k-th compressor, and N_c is the number of active compressors. The derivative of density with respect to pressure is calculated via REFPROP.

A typical pack configuration in a small store consists of scroll compressors that operate in FIFO cycling mode – more compressors kick in once the level of suction pressure reaches a specified upper boundary. In case of fixed volume compressors, the pattern of the active power profile resembles the profile of superimposed duty cycles of all compressors in a pack and the level of load is proportional to the number of working compressors. Active power is calculated based on the enthalpy differential and the rate at which the refrigerant is displaced [32].

$$\dot{W}_c = \frac{1}{\eta_{me}} \dot{V}_d \rho_s (h_{oc} - h_{ic}) \tag{13}$$

where η_{me} is the mechanical efficiency, h_{ic} is the enthalpy at the compressor inlet, h_{oc} is the enthalpy at the compressor outlet, and $\dot{V}_d$ is the total volume displacement rate. Isentropic efficiency $\eta_{is} = 0.7$ is used to obtain the corrected value of h_{oc} from the ideal process of isentropic compression. The active power for HT and LT compressors is calculated independently. Simulation sampling time is 6 s, while the presented model does not include condenser dynamics and assumes full condensation with 100% liquid return.

4. Tuning with experimental data

A set of experimental data collected during FFR testing at Riseholme Refrigeration Centre was used to tune the model. The test site resembles a typical under 2000 sqft supermarket store with 15 cabinets, 13 chillers (HT) and 2 freezers (LT), and scroll compressor pack with a total of 6 fixed volume compressors, 4 HT and 2 LT. The test site layout is illustrated in Fig. 5.

The suction pressure dynamics in the suction line was measured during experiments at the test site. The procedure consisted of closure of the expansion valves and full shut-down of the compressor pack for 30 min. The experimental data was used to estimate the average rate of gas accumulation in the suction line during the shut-down of the system. An example of the suction pressure dynamics is presented in Fig. 6.

4.1. Cooling cabinets

An example of HT case on hysteresis control is presented in Fig. 3(a), and an illustration of the modulation scheme is given in

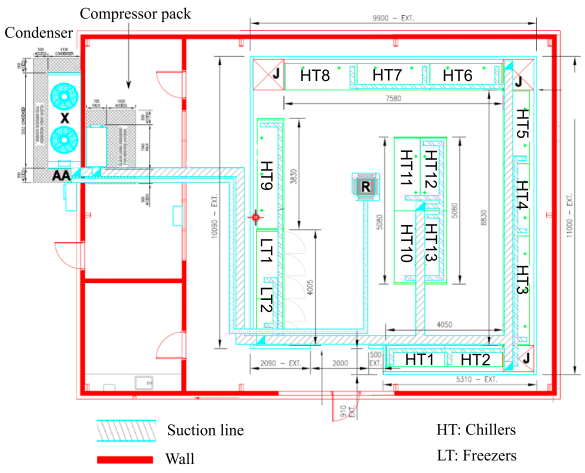

Fig. 5. Test site layout.

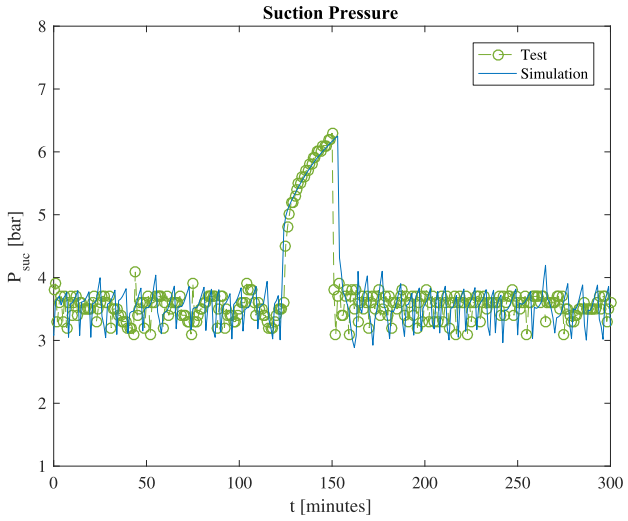

Fig. 6. Pressure dynamics in suction lines during a 30 min full shut-down of the system.

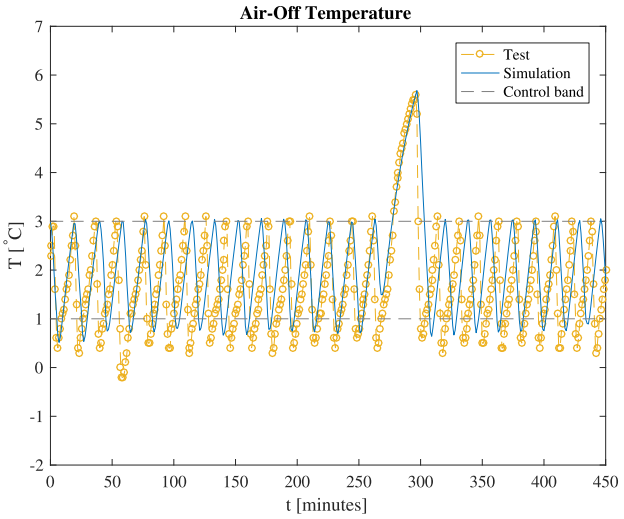

Fig. 7. Temperature time history within a control band.

Fig. 3(b). Here, CPT is the calculated product temperature, a filtered output of the shelf temperature, which is a linear combination of $T_{\text{air}-\text{off}}$ and $T_{\text{air}-\text{on}}$ as follows

$$T_{\text{shelf}} = 0.6T_{\text{air}-\text{off}} + 0.4T_{\text{air}-\text{on}} \tag{14}$$

and CPT at k-th minute being

$$\text{CPT}_k = \frac{1}{30}\left(\sum_{i=1}^{29} \text{CPT}_{k-i} + T^k_{\text{shelf}}\right) \tag{15}$$

where T^k_{shelf} is the shelf temperature at the k-th minute. This induces artificial thermal inertia to the temperature readings from the probes and provides an estimated temperature of foodstuff on the shelves. This notation for CPT and shelf temperature is widely used in commercial refrigeration [33] and is adopted for the presented simulation model. It should be noted that CPT is also calculated for empty cases as no additional information about the shelf contents is used. As 29 previous CPT values are required to calculate a new one on each iteration, when logging starts the first 29 CPT readings are estimated and equal to the corresponding T^k_{shelf} values. Further readings are self-corrected over time.

The tuning of the air temperature values and identification of thermodynamic properties were based on the air-off probe readings and the type of cabinet (Fig. 7). Readings from the air-on probe were dependent on the temperature distribution across the premises, and this dependency was especially profound for refrigeration cases with an air curtain. For simplicity, the indoor ambient temperature was assumed to be the same for all refrigeration cases in the presented model. The set of tuned parameters is $\Omega_{\text{fr}} = [\alpha, \beta, U_{\text{pr}}, A_{\text{pr}}, U_{\text{air}}, A_{\text{air}}, m_{\text{pr}}, m_{\text{air}}, V_s]$. The fitting procedure and parameter estimation were performed using Matlab Optimisation Toolbox (constrained nonlinear minimisation) with a sum of square errors as the objective function.

The test site includes a total of 15 cases: 13 chillers (HT) and 2 freezers (LT). Defrost schedule consists of 4 defrosts per day for HT cabinets and 2 defrosts per day for LT cabinets. Case control set-points (cut-out) vary from -2 to 1 °C for HT cases and set to -23 °C for LT cases with the temperature differential set to 2 °C for all cases. Each case has a total of four probes installed: two placed at the inlet and the outlet of the evaporator coil (S1 & S2), and the other two at the front and the back of the left half of the cabinet (S3 & S4). Temperature control is performed based on the readings from S4 probe for all HT cases and a linear combination of two probes with a ratio of 60% S4 and 40% S3 for LT cases.

4.2. Compressors

A pack of 6 Copeland scroll compressors installed at the test site are used for calibration of the model. All 4 HT compressors are identical ZB45KCE fixed volume displacement machines – scroll compressors, operating only at full capacity. The average active power drawn by a single compressor varies from 3.75 to 4.5 kW. LT compressors are of different size and represented by models ZF09K4E and ZF15K4E. Compressor cycling triggers are determined by the value of suction pressure and the duty time; all compressors have a relay controlled 3 min cool-down period which prevents them from starting frequently. Electrical data is logged on a minute-by-minute basis and stored on an embedded system installed at the test site. An example of a DSR trigger on the pack load is illustrated in Fig. 8.

5. Simulation results

Simulations were performed for a 24-h period with scheduled defrosts occurring 4 times per day for each HT case and twice per day for each LT case. Defrosts are scheduled at different times for each case to minimise undesired overlapping and allow smoother flow of refrigerant in the system.

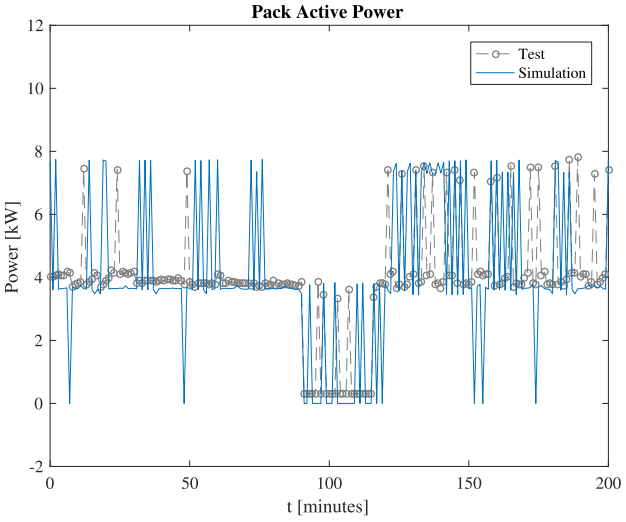

Fig. 8. Active power consumed by HT compressors.

Table 1
Parameter values for two different static FFR scenarios.

Static firm frequency response scenarios		
	FFR 1	FFR 2
Response type	Prim. & Sec.	Secondary
P_s offset	0.6 bar	1.1 bar
Valve closure	Immediately	Immediately
Pack Off/On	Immediately	After 30 s
Duration	30 min	29.5 min

5.1. Systems' response to FFR DSR

The testing procedure is designed to examine different scenarios of system operation in response to FFR DSR. As, for food safety, some cases will have to continuously operate through a FFR event, the authors tested the hypothesis that a safe approach to reduce pack compressor function that minimises engineering risk (caused by a potential flow of liquid refrigerant back into the compressor) requires an immediate offset of the suction pressure set point. This allows limited but continuous flow of refrigerant through the system and ensures that refrigeration is not disrupted for cases that for food safety reasons (food temperature exceeds set point) cannot be switched off during the FFR event. A very common example of this is when cases are recovering from defrost. We simulated two FFR scenarios presented in Table 1.

The offset for the first FFR simulation (FFR1, $t = 100$) is 0.6 bar, increasing the reference value of suction pressure from 3.4 to 4.0 bar for the HT system and from 0.7 to 1.3 bar for the LT system to assure the conservative operation of compressor pack without compromising cooling capacity of all remaining cases. The offset for the second FFR simulation (FFR2) is set to 1.1 bar ($t = 700$). The choice of the suction pressure offset values and its effect on evaporation temperature is discussed by the authors in [34]. In FFR1 the compressor pack is switched off for the first 30 s to ensure the load is shed instantly during the primary response, and then switched back on with the suction pressure offset applied for the duration of the event to make the system perform conservatively while compressing the remaining refrigerant in the suction lines. For the second simulation, FFR2, the pack is switched off 30 s later, omitting the primary response, to allow some time for the remaining gas to safely leave the suction line and therefore remove the risk that the refrigerant condenses and damages the compressor. The FFR2 scenario can also represent DSR tenders that only call for the secondary response, typically 30 s after the grid frequency has dropped

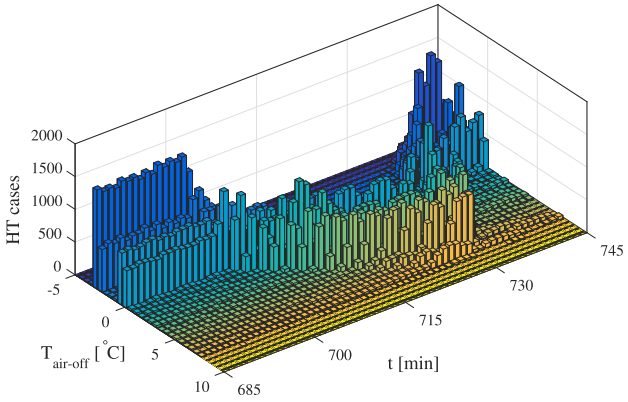

Fig. 10. $T_{air-off}$ temperature evolution of HT cases following FFR DSR triggered at $t = 700$.

to the trigger level. Accumulation of the refrigerant in the evaporator coil and valve opening is presented in APPENDIX for the two different control schemes (FFR1 and FFR2).

In these scenario during an FFR event a HT case receives refrigerant when it reach a pre-defined temperature threshold (8 °C on the air-off probe). After an FFR event the entire system has to be cooled-down, and the load increases significantly to bring all cases back to normal temperature levels.

5.2. Aggregated power profile

Aggregated loads from 300 compressor packs were determined (Figs. 9 and 10). The packs in the network can be treated independently, and aggregated loads are representative of a portfolio of 300 small stores with an assumption that they all operate at the same level of discharge pressure and there is 100% liquid return to the receiver. Simulations of aggregated loads from 300 packs with HT cases on hysteresis control are presented in Fig. 9(a) for both HT and LT compressors. It can be seen that the active power oscillates as the system recovers post FFR. The oscillation is convergent as defrost schedules of each pack contribute to reshuffling of the temperature profiles over time, providing a damping effect to the synchronisation. It can also be noted in Fig. 9(a) that shortly after shut down there is a power spike induced by the remaining refrigerant in HT suction line. The total flow of refrigerant in LT suction lines is smaller compared to the flow in HT suction lines, as there are only two freezers in each

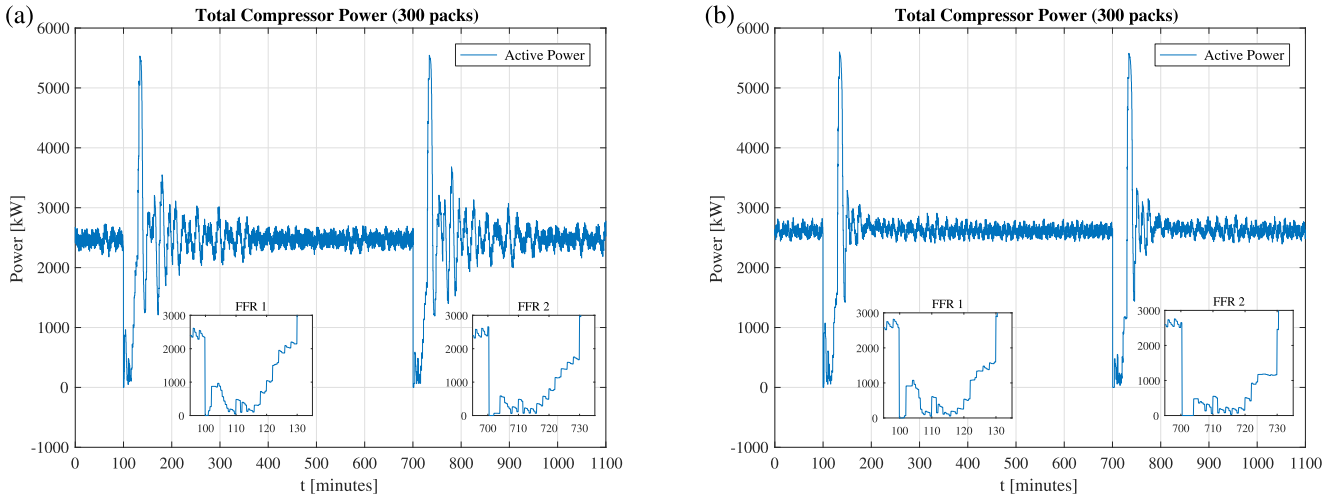

Fig. 9. Modelling of an aggregated power profile of 300 packs following FFR DSR. $T_{amb} = 20$ °C. (a) HT cases are on hysteresis control; (b) HT cases are on modulation control.

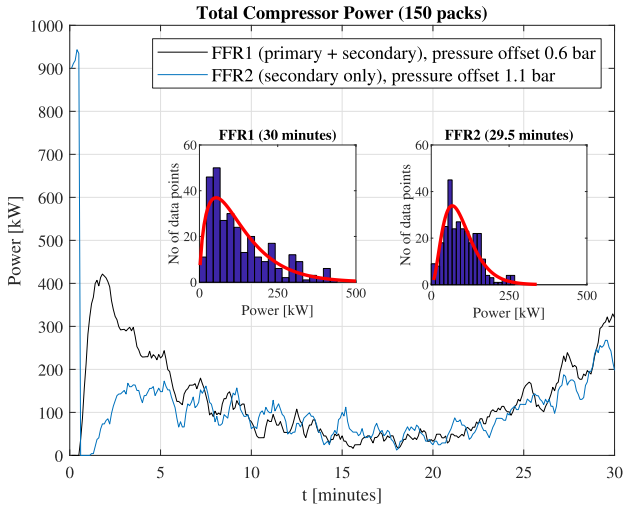

Fig. 11. Transients associated with the remaining refrigerant in the system, $t \in (0, 10)$, and the refrigeration cases switching back on, $t \in (20, 30)$; the data distribution fits are included for both FFR scenarios.

system. An aggregated response of 300 packs with HT cases on modulation control is presented in Fig. 9(b). The profound oscillations are not present in the power profile when the cases are on modulation control, but it can be seen that periodic disturbances persist in the time series. Temperature evolution for all HT assets is presented in Fig. 10.

6. Results and discussion

The simulation of an aggregated response to FFR with a network of fixed volume compressor packs illustrates two important transients associated with the flow of refrigerant in the system when FFR triggers. Fig. 11 shows the first transient (0–10 min) of reducing pack load as the compressors, with a new offset suction pressure work, work on refrigerant trapped between the outlets of the expansion valves and the inlets of the compressor packs. Once boiled in evaporator coils, the refrigerant travels to suction lines; the second transient (20–30 min) is a consequence of refrigeration cases calling for increased cooling as food temperature increases with time through the FFR. Both transients are further illustrated in Figs. 12 and 13 as a function of the valve control scheme and FFR scenario. The total power drawn by HT compressors is plotted against the average temperature of all HT cases. In the FFR1 scenario simulation, Fig. 12(a), the average active power during FFR is

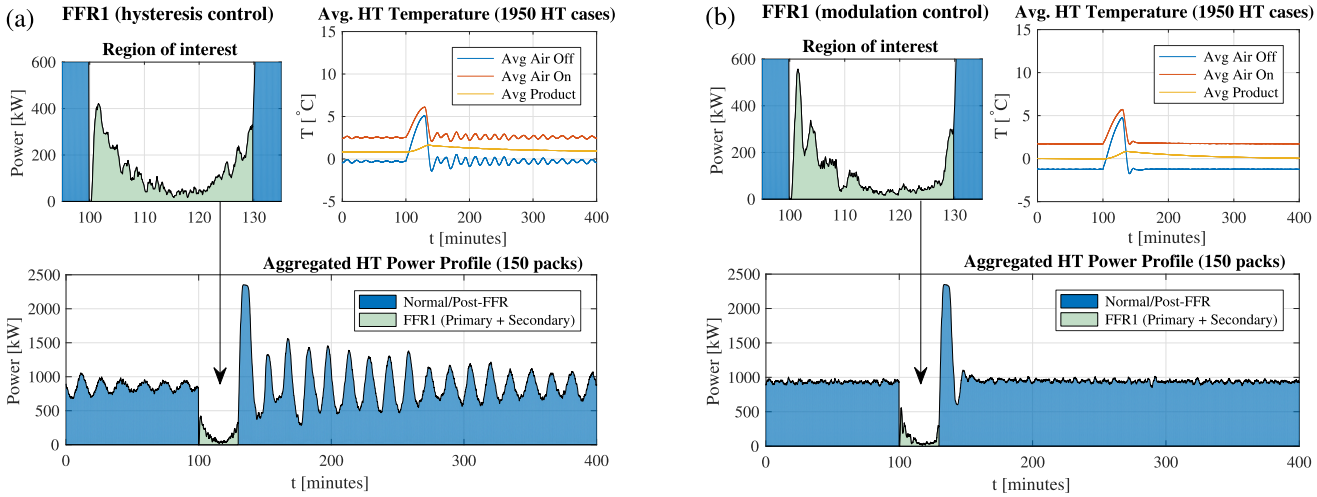

Fig. 12. T_{amb} = 15 °C. Modelling of an aggregated power profile of 150 packs following primary and secondary FFR response (FFR1) triggered at t = 100. Suction pressure offset is 0.6 bar. (a) HT cases are on hysteresis control; (b) HT cases are on modulation control.

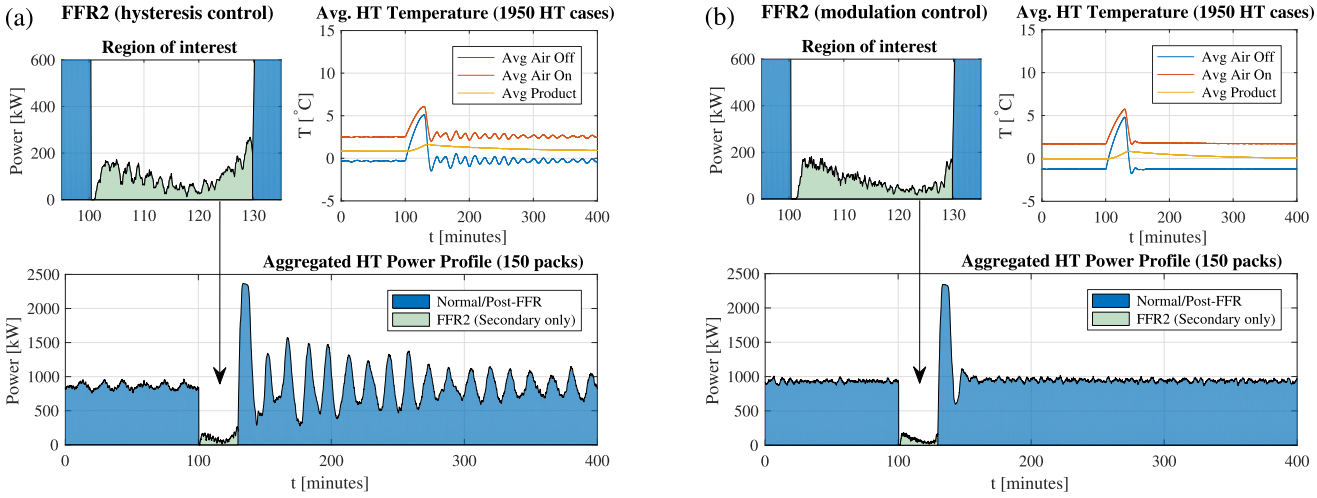

Fig. 13. T_{amb} = 15 °C. Modelling of an aggregated power profile of 150 packs following secondary FFR response (FFR2) triggered at t = 100. Suction pressure offset is 1.1 bar. (a) HT cases are on hysteresis control; (b) HT cases are on modulation control.

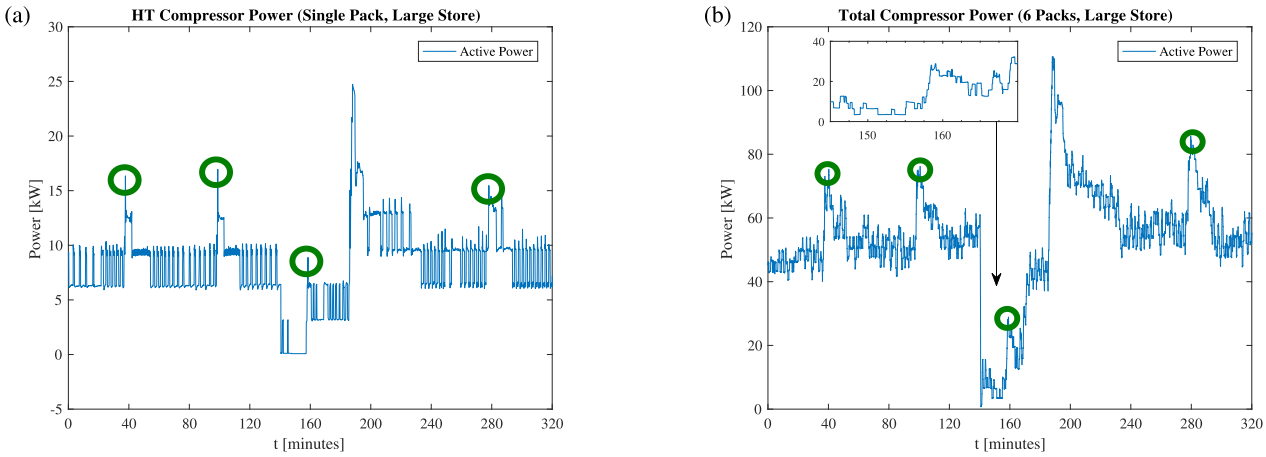

Fig. 14. Experimental data from pack submeters and data loggers at a large store. (a) Power profile of a single HT pack. Green circles highlight power spikes associated with c.24% of all HT refrigeration cases on simultaneous post-defrost pull-down each hour; (b) Power profile of 6 packs with overlapping defrosts resulting in hourly power spikes.

129.21 kW, and the RMS of active power is 99.33 kW. In the FFR2 simulation shown in Fig. 12(b), the average active power during FFR is 111.91 kW with the RMS higher than the average (112.09 kW). Baseline is calculated over the period $t \in [40, 100]$ and is 859.24 kW and 932.4 kW correspondingly. For both FFR1 and FFR2 scenario, modulation controlled showed a dramatic reduction in power oscillations post FFR compared to hysteresis control.

The choice of the suction pressure offset is a trade-off between the evaporation temperature and the power drawn by compressors. High suction pressure set-point will reduce the cycling of compressors and contribute to load reduction in the system. This, however, as previously investigated by the authors in [34], will impact the cooling capacity of refrigeration cases that cannot be switched off and participate in FFR event due to food safety considerations.

In FFR2, where only secondary FFR is considered and a higher value of suction pressure offset is applied (1.1 bar), it is possible to reduce the power associated with compression of the remaining refrigerant. In Fig. 13(a), the average active power during FFR is 97.19 kW, and the RMS of active power is 53.88 kW. For the modulation control scheme shown in Fig. 13(b), the average active power during FFR is 78.45 kW, and the RMS of active power is 44.79 kW. Baseline is calculated over the period $t \in [40, 100]$ and is 861.56 kW and 930.98 kW correspondingly.

The active power error over a 30 min period of DSR varies significantly depending on the FFR scenario and the chosen control scheme. In Fig. 12(a), the RMS of active power is 13.6% of the load shed from the baseline of normal operation (859.24 kW) to the average under FFR (129.21 W). For scenario FFR1 (Fig. 12(b)), the RMS of active power is 13.66% of the load shed from the baseline of normal operation of 932.4 kW to an average under FFR of 111.91 kW. For FFR2 (Fig. 13(a)), the RMS of active power is 7.05% of the load shed from the baseline of normal operation of 861.56 kW to the average under FFR of 97.19 kW. For FFR2 under modulation control, Fig. 13(b), the RMS of active power is 5.25% of the load shed from the baseline of normal operation of 930.98 kW to the average under FFR of 78.45 kW.

Different strategies can be investigated to mitigate these transient responses. In real conditions, every pack will have a subset of refrigeration cases that cannot be switched off, which means a limited refrigerant flow will always be present in the system. Availability of these cases, however, changes over time and more cases can be added to the set of available ones as a refrigeration estate passes through the DSR, partially compensating for those that can no longer remain in an off state since they have reached the critical food safety temperature (as in Fig. 13). Here and further in the text, by refrigeration estate the authors mean the distributed network of commercial refrigeration assets available for participation in frequency balancing services and connected to a smart grid.

6.1. Defrost schedules and hourly power spikes

Tests were conducted in a live superstore to validate the approach. Actual second by second data collected from submeters in the large operational retail store with 6 compressor packs show that overlapping of defrost cycles periodically increases the flow of refrigerant to suction lines during simultaneous FFR pull-downs of refrigeration cases. This can be seen in Fig. 14(a), where the power fluctuates rising up to around 50% above the baseline even under normal operation and even when aggregated from all 6 packs Fig. 14(b). This overlapping is the result of defrosts being scheduled at the beginning of each hour for a considerable amount of refrigeration cases (c.24% of all HT cases are entering defrost each hour). As such power spikes may result in an undesired increase in power consumption during FFR, in the simulation model the authors generate defrost schedules specific for each compressor pack and refrigeration cases assigned to it. Refrigeration cases that have already entered defrost may terminate their state in the middle of the load shedding event if they reach the end of the defrost cycle, and shifting each defrost schedule by 5 min for each subsequent

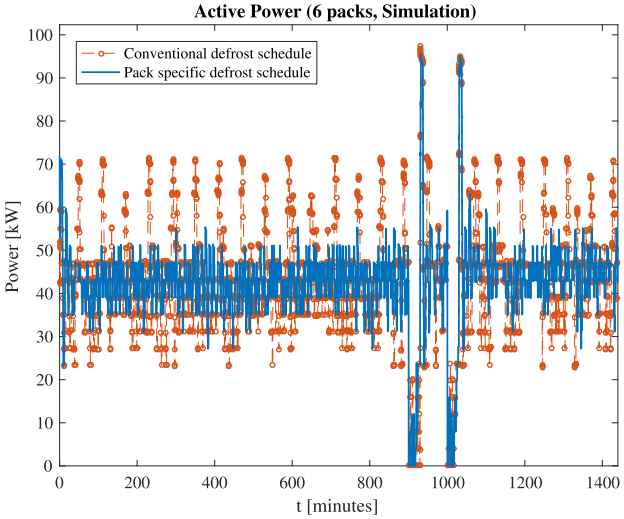

Fig. 15. Conventional defrost schedule (in orange) and defrost schedule generated separately for each pack to eliminate hourly power spikes (in blue).

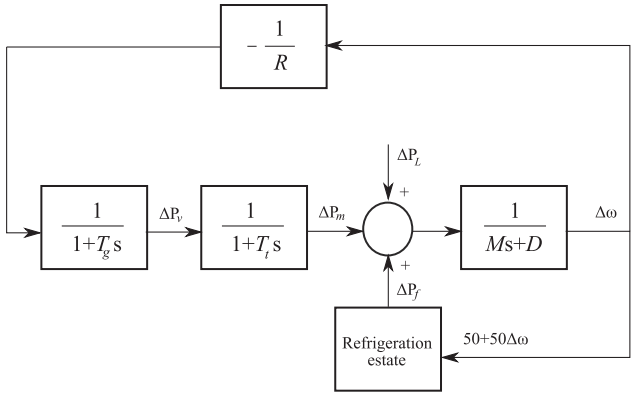

Fig. 16. Power grid model.

pack in the network allows to iron out the power consumption, when multiple packs are aggregated, as shown in Fig. 15. It should be noted that this shift is performed beforehand at the scheduling stage for all cases participating in the frequency response event.

6.2. Connection to the grid model

Here, the authors link the simulation model of refrigeration loads to a simplified power grid model proposed in.

[35] and widely used in the literature for modelling the frequency response [36,37]. The grid model used in this paper is a third-order state space model utilising the generator droop control with the equivalent gain R. The model block diagram is presented in Fig. 16, where T_g is the governor time constant, T_t is the turbine time constant, and M and D are the system's inertia and damping correspondingly. The deviation of the power consumed by refrigeration estate is presented by ΔP_f (it is assumed that no additional loads are linked to the grid). The power loss injection profile that is used to model an incident is presented by ΔP_L. This representation yields a state vector $\mathbf{x}_t = [\Delta P_v, \Delta P_m, \Delta\omega]^T$ for the system $\dot{\mathbf{x}}_t = A\mathbf{x}_t + Bu_t$ with state and input matrices as follows

$$A = \begin{pmatrix} -\frac{1}{T_g} & 0 & -\frac{1}{RT_g} \\ \frac{1}{T_t} & -\frac{1}{T_t} & 0 \\ 0 & \frac{1}{M} & -\frac{D}{M} \end{pmatrix} \tag{16}$$

$$B = \begin{pmatrix} 0 \\ 0 \\ -\frac{1}{M} \end{pmatrix} \tag{17}$$

and the input $u_t = (\Delta P_f + \Delta P_L)/P_{tot}$, where $P_{tot} = 50$ GW is the total power supplied by the network.

The grid model parameter values are adopted from [38,12]. An incident resulting in a loss of 1.32 GW of power for 15 min with subsequent recovery to normal operation over the next 10 min is simulated and the FFR event is triggered within refrigeration estate when the frequency drops below 49.7 Hz.

The response includes both primary and secondary time-scale to arrest the frequency drop and contribute to its recovery once the nadir is reached. Both the power loss injection profile and the aggregated response with a delay are presented in Fig. 17(a). The refrigeration response was scaled up to represent the aggregated load of over 100 MW. It can be seen that the load shifted to a post-FFR region (time interval from 4000 to 5000) to cool back refrigeration assets may contribute to triggering another FFR event. In Fig. 17(b) a peak shaving method is presented that exploits the temperature pull-down duration by extending it in order to avoid immediate power spike. This is achieved by dynamically adjusting the suction pressure offset for the next 30 min back to its set-point value. Frequency response is presented in Fig. 18 for both types of refrigeration response, without and with peak shaving. It can be seen that the aggregated loads can provide considerable frequency restoration potential, but the load shift is also capable of causing a subsequent mismatch between supply and demand, potentially causing another frequency event as shown in Fig. 18(a) in the region from 4000 to 5000, when the estate is consuming additional power to return the fridge network to normal operation. In contrast to domestic refrigeration loads where controllers are typically limited to maintaining the temperature within certain boundaries, commercial refrigeration systems can be controlled by adjusting the set-point of the suction pressure which allows variation in the cooling capacity of all refrigeration cases assigned to a specific pack. This is illustrated in Fig. 18(b) where the frequency response is shown for the refrigeration estate with cooling capacity dynamically adjusted for an additional 30 min by gradually decreasing the suction pressure.

7. Conclusions and future directions

7.1. Conclusions

In this paper, the authors present a novel control mechanism to

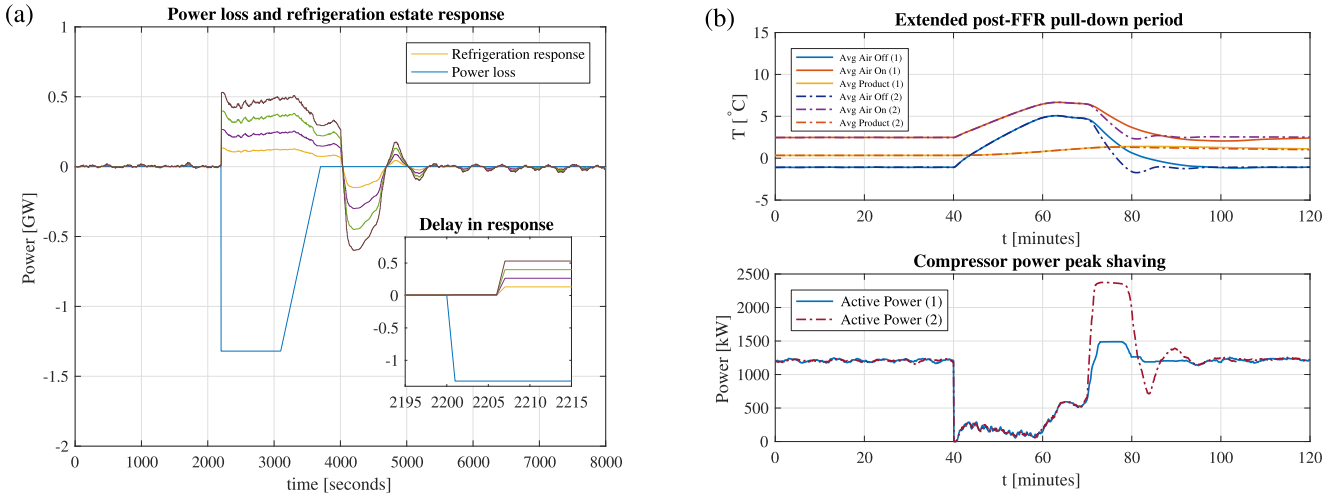

Fig. 17. (a) A sudden loss of over 1GW of power and delayed response from the refrigeration estate; (b) eliminating the spike in power consumption by gradually reducing the suction pressure offset to extend the temperature pull-down period.

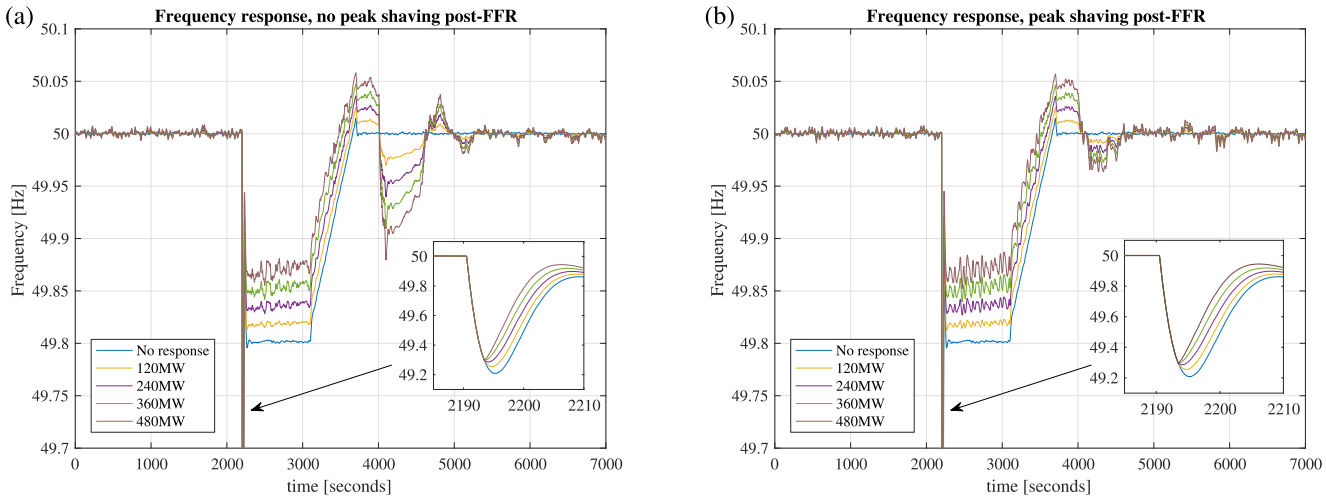

Fig. 18. Frequency response without and with peak shaving.

aggregate massive networks of commercial refrigeration systems for use in frequency balancing services that both minimises engineering and food safety risk. We simulated a 30 min firm frequency response event that has been triggered for populations of 150 and 300 compressor packs, based on a validated mathematical model of a commercial refrigeration system with 6 fixed speed compressors and 15 refrigeration cases. The model was tuned with experimental data obtained from the Riseholme Refrigeration Research Centre to resemble a typical under 2000 sqft supermarket store. The system was then replicated with randomised initial conditions and new defrost schedules to minimise fluctuations in aggregated loads. The system's response to a frequency drop was presented for two control schemes of expansion valve operation, hysteresis and modulation. Valves on hysteresis control exhibited synchronisation behaviour post-event with oscillations in the power time series converging over time due to cases entering new defrosts. Transient response of the system during the load shedding event showed significant fluctuation of active power when the system responds to primary and secondary parts of the event. The proposed scenario of delivering the response is on a secondary scale only, by omitting the primary part in its entirety to allow time for compressors to remove gas from the suction lines. Delivering firm frequency response as virtual defrost may result in refrigeration cases existing in a defrost-like state by reaching a pre-defined temperature threshold before the end of a 30 min event, thus requiring more cases to be added in order to compensate the load. The refrigeration estate was linked to a power grid model, and an incident resulting in a loss of over 1 GW of power was simulated. It was shown that the load shifting without peak shaving after the event may contribute to a subsequent mismatch between supply and demand that may lead to another drop in frequency. Dynamic suction pressure control is recommended to allow control over the temperature pull-down duration in order to avoid spikes in power consumption during system's return to normal operation.

7.2. Future directions

In addition to the implementation of a centralised iIOT control system to coordinate the control of a national network, the use of variable frequency drives (VFD) to the master compressor would ensure the capacity of compressor is adjusted by varying motor speed when DSR signal arrives. The authors are investigating the potential of VFDs, in the context of DSR, to even the load across the duration of DSR event. Dynamic frequency response based on continuous suction pressure control similar to the strategies proposed for domestic refrigeration in [17,11] and for heat pumps in [18], that utilize dynamic frequency trigger described by linear slopes and parabolic curves correspondingly, is also to be investigated.

Moreover, cold energy storage mechanisms such as ice bank technology are capable of reducing the amount of refrigerant that is required to sustain a fixed level of cooling capacity, thus reducing energy usage by refrigeration systems. By performing additional subcooling of refrigerant after heat rejection in a condenser, it is possible to decrease the enthalpy of the refrigerant as it passes through the expansion device into the evaporator. This will result in an increase of the enthalpy differential as the refrigerant boils in the evaporator, and the same amount of cooling will require a reduced mass flow through the evaporator coil. Additional subcooling could be achieved by diverting the refrigerant through a heat exchanger within a pre-cooled cold storage vessel. Cold energy storage could be utilized during the secondary frequency response by providing additional capacity to keep food product within safe temperature limits.

Note. This paper is an extended version of earlier work presented by the authors in [39]. Different scenarios of delivering firm frequency response are proposed. The refrigeration model is linked to a linear power grid model and a simulated frequency response event is triggered for the coupled system. The sampling frequency is 10 times of that in the original work to observe the transient response in more detail by capturing all compressor activations within the frequency response region.

Acknowledgment

This research is supported by Innovate UK (Grant No. 102626). The authors would like to thank Tesco, IMS Evolve, Global Smart Transformations Ltd and ECH Engineering.

The authors would also like to express their gratitude to Mr. L. Harpham (IMS Evolve), Mr. D. Botting (Global Smart Transformations) and Dr. E.C. Hammond (ECH Engineering) for their guidance and advice during field experiments at the Riseholme Refrigeration Research Centre.

Appendix A

The operation of a single refrigeration case (HT and LT) and a single pack system is illustrated in Fig. 19.

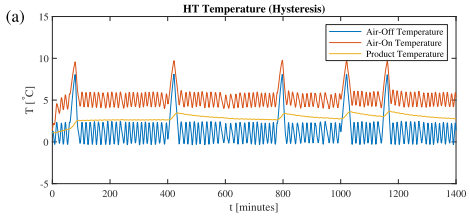

(a) (color online) Simulation of systems' response to FFR triggered at $t = 400$ (FFR1) and $t = 1000$ (FFR2) for 30 minutes: temperature profile of an HT system on hysteresis control.

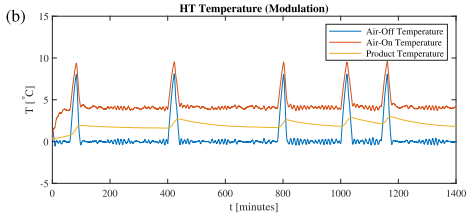

(b) (color online) Simulation of systems' response to FFR triggered at $t = 400$ (FFR1) and $t = 1000$ (FFR2) for 30 minutes: temperature profile of an HT system on modulation control.

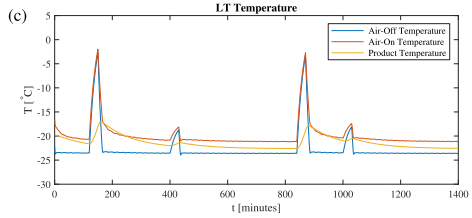

(c) (color online) Simulation of systems' response to FFR triggered at $t = 400$ (FFR1) and $t = 1000$ (FFR2) for 30 minutes: temperature profile of an LT system. Higher temperature spikes during defrost are due to operating heaters.

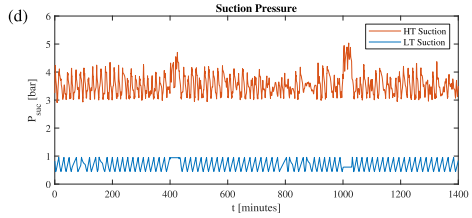

(d) (color online) Simulation of systems' response to FFR triggered at $t = 400$ (FFR1) and $t = 1000$ (FFR2) for 30 minutes: HT and LT suction pressure.

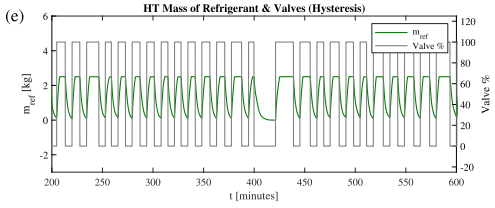

(e) (color online) Simulation of systems' response to FFR1 triggered at $t = 400$ for 30 minutes (zoomed in to the area of interest): (a) Valve state and mass of refrigerant in the coil (hysteresis); (b) Valve state and mass of refrigerant in the coil (hysteresis).

Fig. 19. Single pack system.

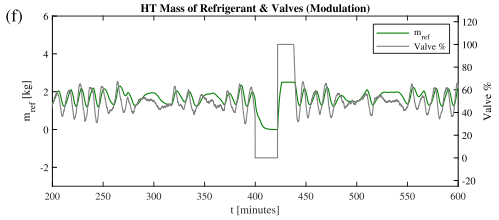

(f) (color online) Simulation of systems' response to FFR1 triggered at $t = 400$ for 30 minutes (zoomed in to the area of interest): (a) Valve state and mass of refrigerant in the coil (hysteresis); (b) Valve state and mass of refrigerant in the coil (modulation).

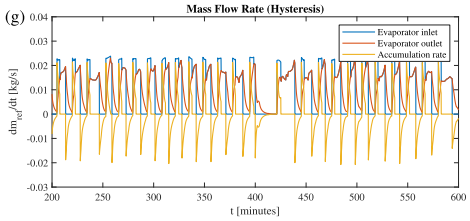

(g) (color online) Simulation of systems' response to FFR1 triggered at $t = 400$ for 30 minutes (zoomed in to the area of interest): Mass flow rate at evaporator inlet (blue), outlet (red) and accumulation rate of refrigerant in the coil (yellow) for hysteresis control.

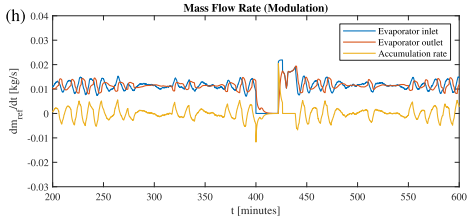

(h) (color online) Simulation of systems' response to FFR1 triggered at $t = 400$ for 30 minutes (zoomed in to the area of interest): Mass flow rate at evaporator inlet (blue), outlet (red) and accumulation rate of refrigerant in the coil (yellow) for modulation control.

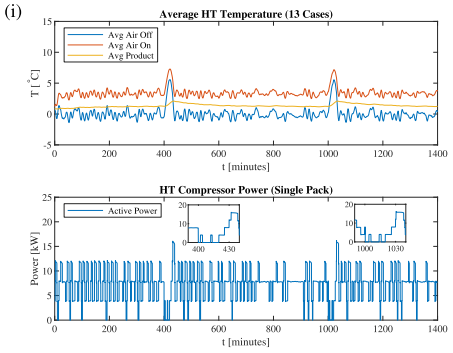

(i) (color online) Simulation of HT systems' response to FFR triggered at $t = 400$ (FFR1) and $t = 1000$ (FFR2) for 30 minutes. Hysteresis control, $T_{\text{amb}} = 20^{\circ}\text{C}$.

Fig. 19. (*continued*)

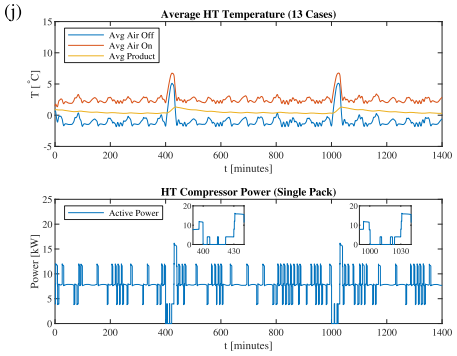

(j) (color online) Simulation of LT systems' response to FFR triggered at $t = 400$ (FFR1) and $t = 1000$ (FFR2) for 30 minutes. Modulation control, $T_{\text{amb}} = 20°\text{C}$.

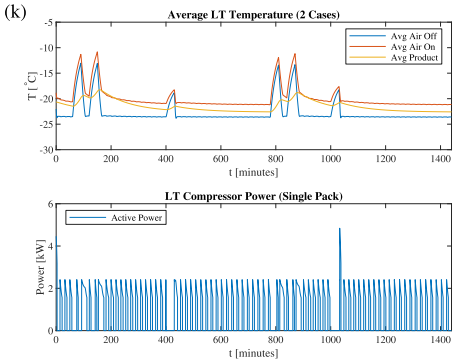

(k) (color online) Simulation of LT systems' response to FFR triggered at $t = 400$ (FFR1) and $t = 1000$ (FFR2) for 30 minutes.

Fig. 19. (*continued*)

References

[1] Bradley P, Coke A, Leach M. Financial incentive approaches for reducing peak electricity demand, experience from pilot trials with a UK energy provider. Energy Policy 2016;98:108–20.

[2] Grünewald P, Torriti J. Demand response from the non-domestic sector: early UK experiences and future opportunities. Energy Policy 2013;61:423–9.

[3] Granell R, Axon CJ, Wallom DC, Layberry RL. Power-use profile analysis of non-domestic consumers for electricity tariff switching. Energy Eff 2016;9(3):825–41.

[4] Firm frequency response FAQ. In: Version 1.3, National Grid; August 2017. p. 1–14.

[5] Smethurst K, Hynes H, Rook-Grignon O, Walsh V. Testing guidance for providers of firm frequency response balancing service Version D11; 2017.

[6] Teng F, Aunedi M, Pudjianto D, Strbac G. Benefits of demand-side response in providing frequency response service in the future GB power system. Front Energy Res 2015;3:36.

[7] Morales González R, Shariat Torbaghan S, Gibescu M, Cobben S. Harnessing the flexibility of thermostatic loads in microgrids with solar power generation. Energies 2016;9(7):547.

[8] Qadrdan M, Cheng M, Wu J, Jenkins N. Benefits of demand-side response in combined gas and electricity networks. Appl Energy 2017;192:360–9.

[9] Tassou SA, Kolokotroni M, Gowreesunker B, Stojceska V, Azapagic A, Fryer P, et al. Energy demand and reduction opportunities in the UK food chain. Proc Inst Civil Eng-Energy 2014;167(3):162–70.

[10] Kremers E, Marı J, Barambones O, et al. Emergent synchronisation properties of a refrigerator demand side management system. Appl Energy 2013;101:709–17.

[11] Short JA, Infield DG, Freris LL. Stabilization of grid frequency through dynamic demand control. IEEE Trans Power Syst 2007;22(3):1284–93.

[12] Angeli D, Kountouriotis P-A. A stochastic approach to "dynamic-demand" refrigerator control. IEEE Trans Control Syst Technol 2012;20(3):581–92.

[13] Borsche TS, de Santiago J, Andersson G. Stochastic control of cooling appliances under disturbances for primary frequency reserves. Sust Energy Grids Networks 2016;7:70–9.

[14] Braun M, Altan H, Beck S. Using regression analysis to predict the future energy consumption of a supermarket in the UK. Appl Energy 2014;130:305–13.

[15] Rasmussen LB, Bacher P, Madsen H, Nielsen HA, Heerup C, Green T. Load forecasting of supermarket refrigeration. Appl Energy 2016;163:32–40.

[16] Stadler M, Krause W, Sonnenschein M, Vogel U. Modelling and evaluation of control schemes for enhancing load shift of electricity demand for cooling devices. Environ Model Software 2009;24(2):285–95.

[17] Infield DG, Short J, Horne C, Freris LL. Potential for domestic dynamic demand-side management in the UK. In: Power engineering society general meeting, 2007. IEEE; 2007. p. 1–6.

[18] Muhssin MT, Cipcigan L, Jenkins N, Slater S, Cheng M, Obaid Z. Dynamic frequency response from controlled domestic heat pumps. IEEE Trans Power Syst 2018.

[19] Fayazbakhsh M, Bagheri F, Bahrami M. An inverse method for calculation of thermal inertia and heat gain in air conditioning and refrigeration systems. Appl Energy 2015;138:496–504.

[20] Larsen LFS. Model based control of refrigeration systems. Department of Control Engineering, Aalborg University; 2006.

[21] Shafiei SE, Rasmussen H, Stoustrup J. Modeling supermarket refrigeration systems for demand-side management. Energies 2013;6(2):900–20.

[22] Sarabia D, Capraro F, Larsen LF, de Prada C. Hybrid NMPC of supermarket display cases. Control Eng Pract 2009;17(4):428–41.

[23] Petersen LN, Madsen H, Heerup C. Eso2 optimization of supermarket refrigeration systems. Technical University of Denmark, Department of Informatics and Mathematical Modeling, Tech Rep; 2012.

[24] Lemmon EW, Huber ML, McLinden MO. NIST reference fluid thermodynamic and transport properties-REFPROP. NIST standard reference database v9.1; 2013.

[25] Larsen LF, Izadi-Zamanabadi R, Wisniewski R. Supermarket refrigeration system-benchmark for hybrid system control. In: Proc of ECC07; 2007.

[26] Lenger MJ, Jacobi A, Hrnjak P. Superheat stability of an evaporator and thermostatic expansion valve. Tech rep. Air Conditioning and Refrigeration Center. College of Engineering. University of Illinois at Urbana-Champaign; 1998.

[27] Oskarsson S. Evaporator models for operation with dry, wet, and frosted finned surfaces. ASHRAE Trans 1990;96(1):373–80.

[28] Vinther K. Data-driven control of refrigeration systems. Ph.D. thesis, Ph. D. Dissertation, Institure of Electronic Systems, Aalborg University; 2014.

[29] ASHRAE Handbook Refrigeration. SI ed.; 2010.

[30] Thorade M, Saadat A. Partial derivatives of thermodynamic state properties for dynamic simulation. Environ Earth Sci 2013;70(8):3497–503.

[31] Shafiei SE. Control methods for energy management of refrigeration systems, automation & control. Department of Electronic Systems, Aalborg University; 2015.

[32] Ge Y, Tassou S. Mathematical modelling of supermarket refrigeration systems for

design, energy prediction and control. Proc Inst Mech Eng, Part A: J Power Energy 2000;214(2):101–14.
[33] Lawrence JMW. Monitoring refrigeration units. Patent WO1992009977A1; 1992-05-27.
[34] Saleh IM, Postnikov A, Arsene C, Zolotas AC, Bingham C, Bickerton R, et al. Impact of demand side response on a commercial retail refrigeration system. Energies 2018;11(2):371.
[35] Anderson PM, Mirheydar M. A low-order system frequency response model. IEEE Trans Power Syst 1990;5(3):720–9.
[36] Cheng M, Sami SS, Wu J. Benefits of using virtual energy storage system for power system frequency response. Appl Energy 2017;194:376–85.
[37] Muhssin MT, Cipcigan LM, Sami SS, Obaid ZA. Potential of demand side response aggregation for the stabilization of the grids frequency. Appl Energy 2018;220:643–56.
[38] Jones D. Dynamic system parameters for the national grid. IEE Proc-Gener Transm Distrib 2005;152(1):53–60.
[39] Postnikov A, Zolotas A, Bingham C, Saleh IM, Arsene C, Pearson S, et al. Modelling of thermostatically controlled loads to analyse the potential of delivering FFR DSR with a large network of compressor packs. In: European Modelling Symposium (EMS), 2017. IEEE; 2017. p. 163–7.